Electronic Supplementary Material (ESI) for Journal of Materials Chemistry A.

Supporting Information for

Dynamic Compensation of MnOOH to Mitigate the Irregular Dissolution of MnO_2 in Rechargeable Aqueous Zn/MnO_2 Batteries

Guojun Lai,‡[a] Pengchao Ruan,‡[a] Xueting Hu,[a] Bingan Lu,[b] Shuqiang Liang,[a] Yan Tang *[a] and Jiang Zhou *[a]

a. School of Materials Science and Engineering, Hunan Provincial Key Laboratory of Electronic Packaging and Advanced Functional Materials, Central South University, Changsha 410083 China. E-mail: ty_csu@csu.edu.cn; zhou_jiang@csu.edu.cn

b. School of Physics and Electronics, Hunan University, Changsha 410082 China.

‡ These authors contributed equally to the work.

Experimental Section

1. Preparation of Basic Electrolyte and Zn-Ce Electrolyte

The basic electrolyte consists of 2 M $ZnSO_4$ and 0.1 M $MnSO_4$. The Zn-Ce electrolyte consists of the basic electrolyte and $Ce(SO_4)_2$ additive, and the optimal amount of the $Ce(SO_4)_2$ is 0.5 wt%. The $Ce(SO_4)_2$ is added into the basic electrolyte directly and then the mixed solution was stirring for 6 h.

2. Preparation of MnO_2

The MnO_2 electrode was fabricated by a hydrothermal reaction method. Briefly, 0.2 M $KMnO_4$ (15 mL) and 0.08 M $MnSO_4$ (15 mL) were mixed under continuous stirring for 30 min at room temperature. The mixture was loaded into a 50 mL Teflon-lined autoclave and maintained at 160 °C for 12 h. The obtained product was centrifuged, washed thoroughly using water and absolute ethyl alcohol, and dried at 80 ℃ for 10 h. The mass loading of MnO_2 cathode in Zn/MnO_2 battery with the Zn-Ce electrolyte is 1.5 mg (1.05 mg MnO_2 : 0.3 mg carbon black : 0.15 mg PVDF) and the mass loading of MnO_2 cathode in Zn/MnO_2 battery with the basic electrolyte is 1.6 mg (1.134 mg MnO_2 : 0.324 mg carbon black : 0.162 mg PVDF) at 1.0 $A \cdot g^{-1}$. The mass loading of MnO_2 cathode in Zn/MnO_2 battery is 1.44 mg (1.008 mg MnO_2 : 0.288 mg carbon black : 0.144 mg PVDF) at 0.5 $A \cdot g^{-1}$.

3. Materials Characterization

The cathode material, Zn anode and the electrolyte were recorded by the X-ray diffraction (XRD) in the 2θ range of 5°-80° (Rigaku Mini Flex 600 diffractometer, Cu Kα radiation, λ = 1.5418, step size of 0.02° s^{-1}). A FESEM (FEI Nova NanoSEM 230, 10 kV) field emission scanning electron microscope was used to analyze the morphologies and microstructures of samples. Raman spectra were conducted on a spectrophotometer (DXR, Thermo-Fisher Scientific) with a wavelength of 532 nm. X-ray photoelectron spectroscopy (XPS) was recorded on an ESCALAB 250 Xi X-ray photoelectron spectrometer (Thermo Fisher), and the samples

were retrieved for XPS characterization after thorough washing with ethyl alcohol and drying in vacuo at room temperature. The transition-metal concentration on the cathodes was determined by total reflection X-ray fluorescence spectroscopy (TXRF), employing a LAB CENTER XRF-1800.

4. Electrochemical Measurement

The synthesized MnO_2 powder (70 wt%) was utilized for constructing the cathodes by coating the slurry mixed with acetylene black (20 wt%) and polyvinylidene fluoride (10 wt%) onto the stainless-steel wire mesh (SSWM) with the area of 1.13 cm^2, followed by a drying process at 80 °C for 12 h in a vacuum atmosphere. The Zn/MnO_2 batteries consisted of MnO_2 cathode, Zn anode, glass fiber separation, and basic/Zn-Ce electrolyte, which were encapsulated in CR2025 coin cells for electrochemical measurements. The electrochemical performance measurements were examined by a multichannel battery test system (LAND CT2001A, China). The electrochemical performances at high/low temperature were tested via a high/low temperature test box (LAND GT2001B, China). The CV and EIS measurements were carried out on an electrochemical workstation (CHI660E, China).

Figures and Tables

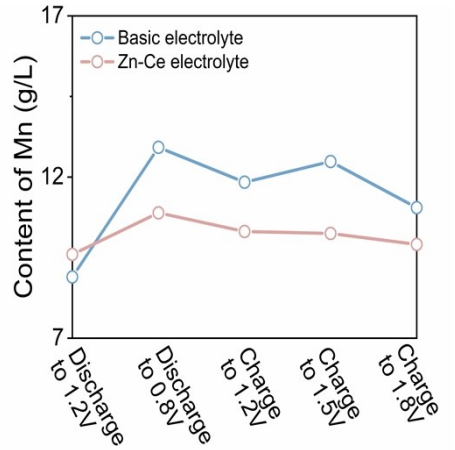

Figure S1 Inductively coupled plasma optical emission spectrometry (ICP-OES) results of the Mn content for the basic/Zn-Ce electrolyte at various charge/discharge states.

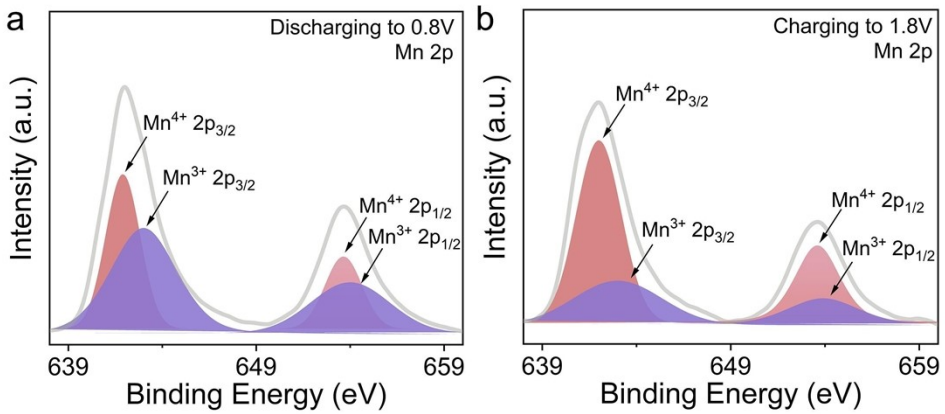

Figure S2 The high-resolution XPS of Mn 2p spectra of the MnO_2 cathode in Zn-Ce electrolyte at different charge/discharge stages.

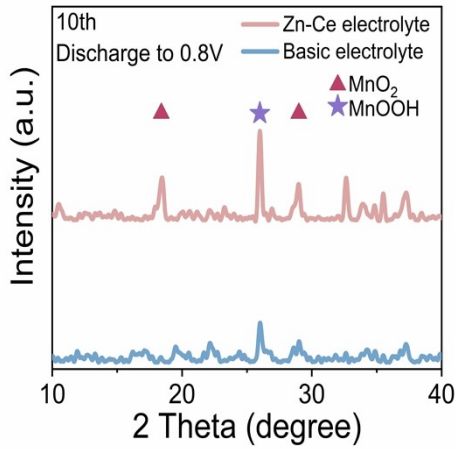

Figure S3 XRD patterns of the MnO_2 cathodes in the basic electrolyte and Zn-Ce electrolyte after 10 cycles and at the stage of discharging to 0.8 V.

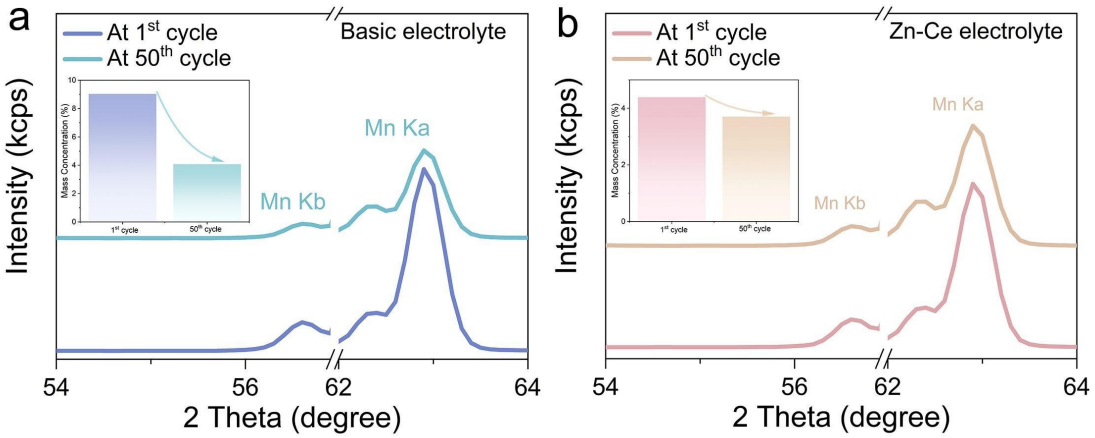

Figure S4 XRF patterns of the MnO_2 cathodes in the basic electrolyte and Zn-Ce electrolyte at 1st cycle and 50th cycle.

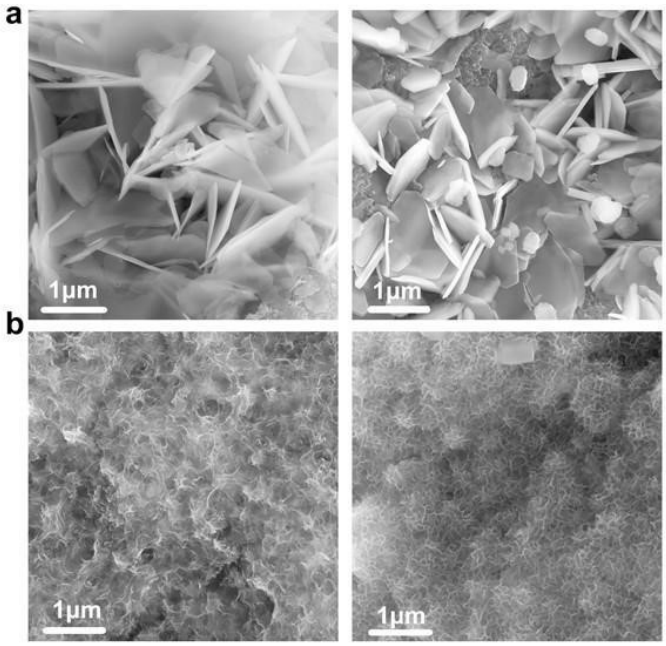

Figure S5 Scanning electron microscopy (SEM) images of MnO_2 cathodes in the basic electrolyte and the Zn-Ce electrolyte at the state of discharging to 0.8 V (left) and charging to 1.8 V (right).

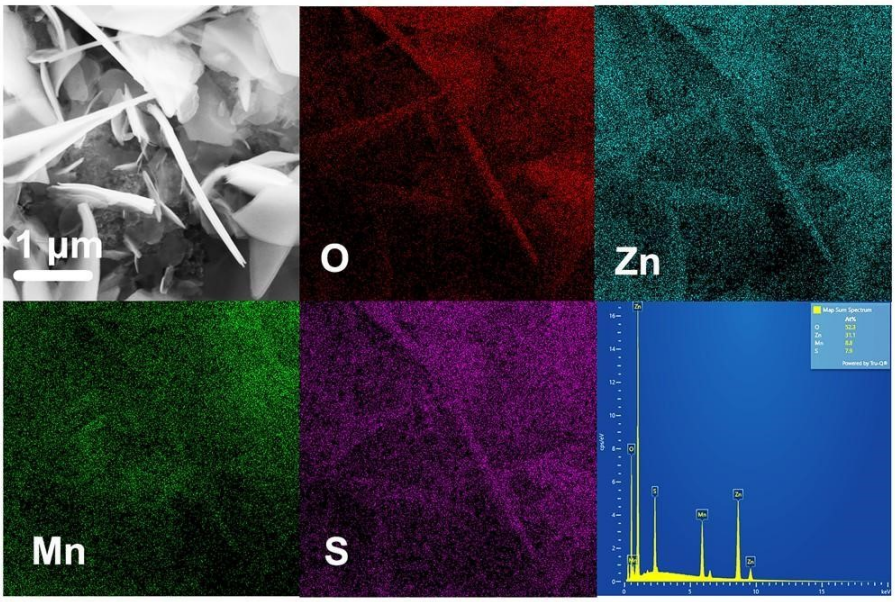

Figure S6 The corresponding elemental mapping images and EDS of the MnO_2 cathode in the basic electrolyte at the state of discharging to 0.8 V.

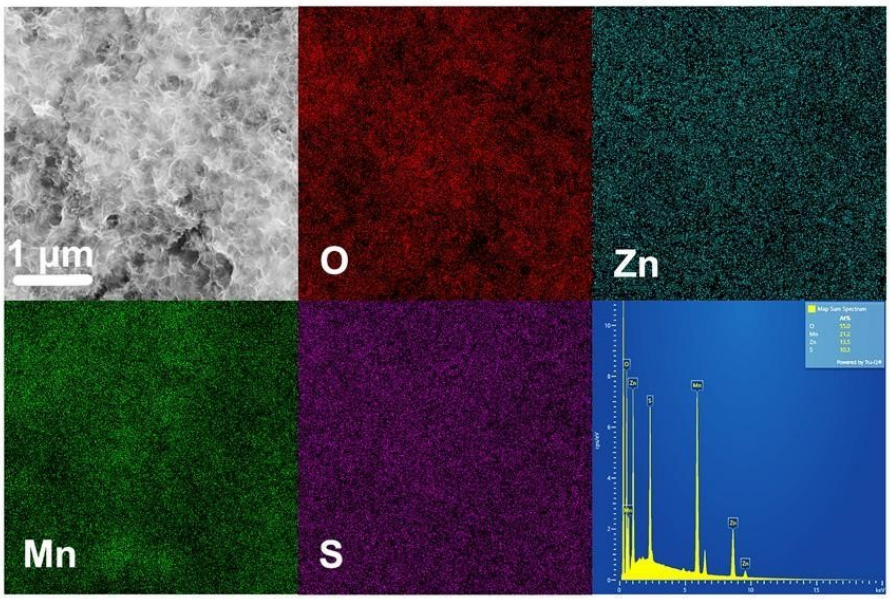

Figure S7 The corresponding elemental mapping images and EDS of the MnO_2 cathode in the Zn-Ce electrolyte at the state of discharging to 0.8 V.

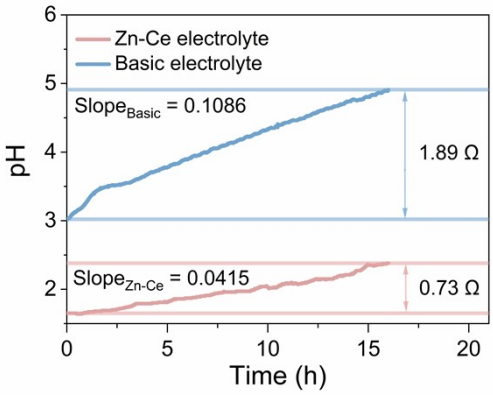

Figure S8 The pH variation of the basic electrolyte and the Zn-Ce electrolyte in the Zn/MnO_2 batteries.

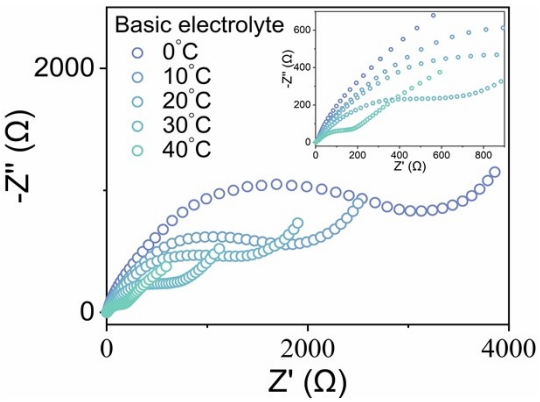

Figure S9 The EIS curves of Zn/MnO_2 batteries with the basic electrolyte at different temperatures.

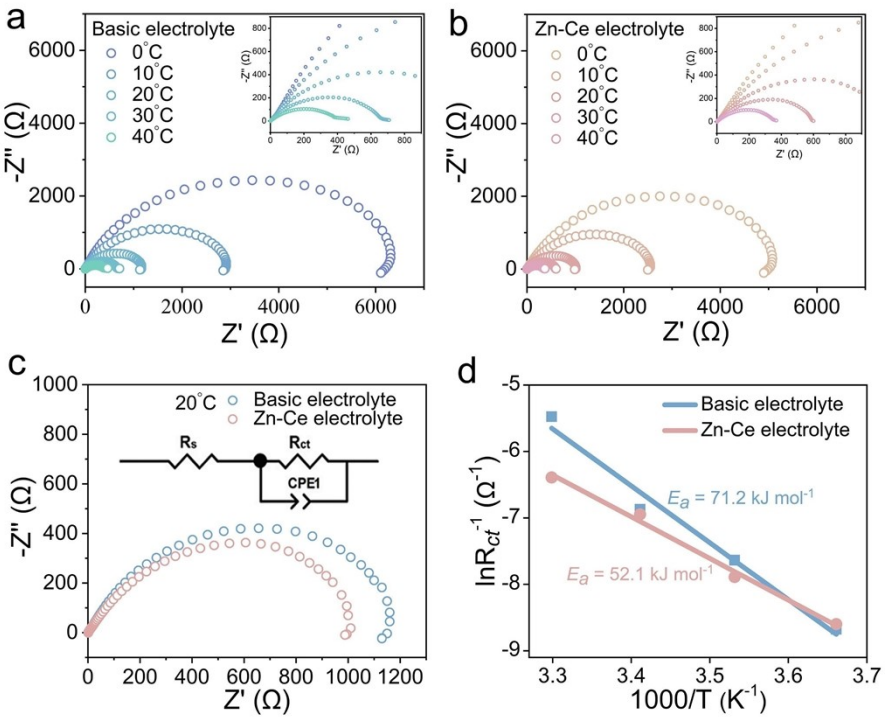

Figure S10 The EIS curves of Zn/Zn batteries with (a) the basic electrolyte and (b) the Zn-Ce electrolyte at different temperatures. (c) The EIS comparison of Zn/Zn batteries with the basic electrolyte and the Zn-Ce electrolyte at 20℃. (d) Arrhenius curves of activation energies (E_a) of Zn/Zn batteries with the basic electrolyte and the Zn-Ce electrolyte.

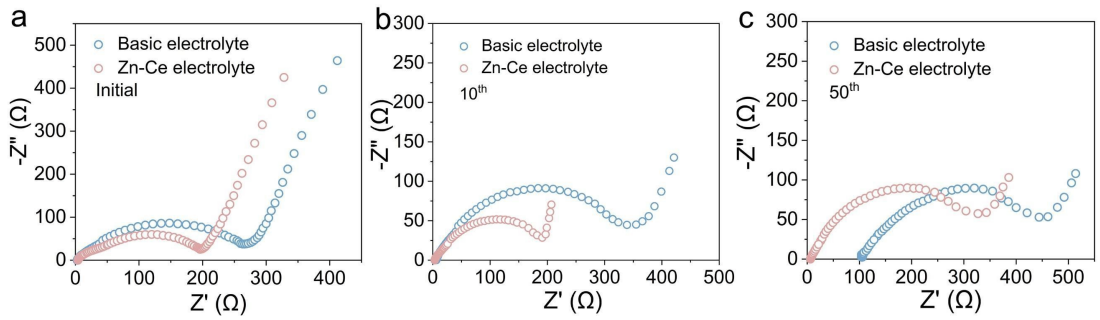

Figure S11 The EIS curves of Zn/MnO_2 batteries with the basic electrolyte and the Zn-Ce electrolyte at a) initial stage, b)10^{th} cycle and c) 50^{th} cycle.

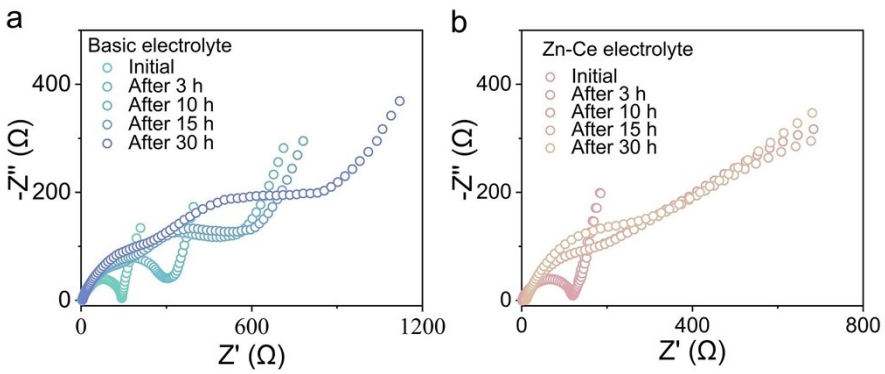

Figure S12 The EIS curves of Zn/MnO_2 batteries with (a) basic electrolyte and (b) Zn-Ce electrolyte at different standing state.

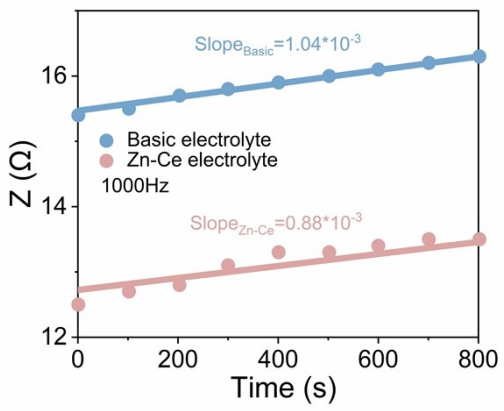

Figure S13 The impendence-time curves of Zn/MnO_2 batteries with the basic electrolyte and Zn-Ce electrolyte at 1000 Hz.

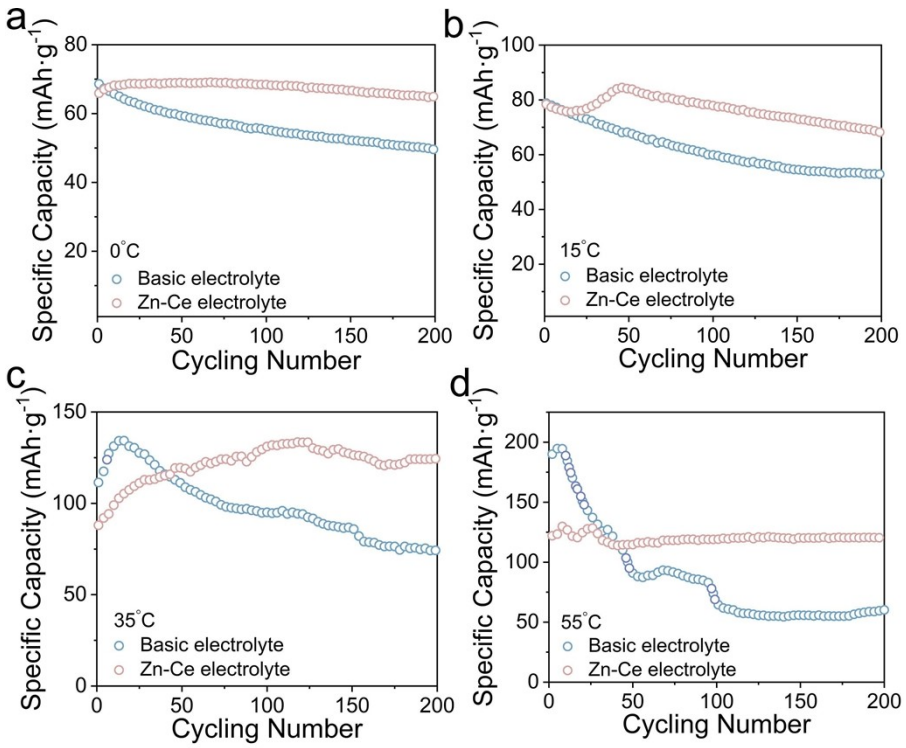

Figure S14 Cycling performances of the Zn/MnO_2 batteries with the basic electrolyte and the Zn-Ce electrolyte in a) 0, b) 15, c) 35 and d) 55℃ at 1 $A \cdot g^{-1}$.

Table S1 Data of R_1 and R_2 for Zn/MnO_2 batteries at different temperatures.

Temperature (℃)	Sample	R_1 (Ω)	R_2 (Ω)
0	Basic electrolyte	2.668	2747
	Zn-Ce electrolyte	1.753	1373
10	Basic electrolyte	2.333	1510
	Zn-Ce electrolyte	1.403	753.6
20	Basic electrolyte	1.983	1157
	Zn-Ce electrolyte	0.551	463.5
30	Basic electrolyte	1.683	608.6
	Zn-Ce electrolyte	1.608	217.0
40	Basic electrolyte	0.971	403.2
	Zn-Ce electrolyte	2.105	154.8

Table S2 Data of R_{ct} and R_S for Zn/Zn batteries at different temperatures.

Temperature (℃)	Sample	R_s (Ω)	R_{ct} (Ω)
0	Basic electrolyte	1.723	6729
	Zn-Ce electrolyte	2.12	5431
10	Basic electrolyte	1.546	3052
	Zn-Ce electrolyte	1.659	2670
20	Basic electrolyte	1.228	1193
	Zn-Ce electrolyte	1.399	1039
30	Basic electrolyte	1.082	671.2
	Zn-Ce electrolyte	1.381	596.3
40	Basic electrolyte	0.971	403.2
	Zn-Ce electrolyte	1.282	351.3

Table S3 The electrochemical performances comparison of Zn/MnO_2 battery based on Zn-Ce electrolyte with other reported Zn/MnO_2 batteries based on the different optimization methods.

Cathode	Electrolyte	Current density ($A \cdot g^{-1}$)	Cycle number	Capacity retention (%)	Ref.
MnO_2	**2 M $ZnSO_4$+ 0.1 M $MnSO_4$+ 0.5 wt% $Ce(SO_4)_2$**	**1.0**	**1000**	**97.4**	**This work**
MnO_2	Solid-state hydrogel electrolyte with three layers (ABC-H)	1.0	1000	93.6	[1]
MnO_2@PEDOT	poly(vinyl alcohol) (PVA)	1.1	300	93.7	[2]
δ-MnO_2 NDs	2 M $ZnSO_4$+ 0.1 M $MnSO_4$	1.0	1000	86.2	[3]
MnO_2	2 M $ZnSO_4$+ 0.1 M $MnSO_4$+ 30 wt% palygorskite	0.5	1000	89.0	[4]
MnO_2	(poly(ethylene glycol) diglycidylether + zinc trifluoromethanesulfonate	0.5	300	85.0	[5]
K^+-intercalated δ-MnO_2	2 M $ZnSO_4$	1.8	100	96.9	[6]
MnO_2 nanorods	1 M $ZnSO_4$	0.2	200	75.0	[7]

Supplementary Discussion

Conversion of Mn^{2+}/MnOOH reaction:

$$Mn^{2+} + Ce^{4+} + 2H_2O \rightarrow MnOOH + Ce^{3+} + 3H^+$$

$\Delta G_0 = \Delta_f G(MnOOH) + \Delta_f G(Ce^{3+}) + 3\Delta_f G(H^+) - [\Delta_f G(Mn^{2+}) + \Delta_f G(Ce^{4+}) + 2\ \Delta_f G(H_2O) =$ -822.6 - 96500*1.72/1000-(-228 -237.2*2) = -286.18 KJ mol^{-1}

$$\Delta G = \Delta G_0 - RTlnQ = 0$$

$$RTlnQ = RTlnln[\frac{c(Ce^{3+}) * c^3(H^+)}{c(Ce^{4+}) * c(Mn^{2+})}]$$

$$ln[\frac{c(Ce^{3+}) * c^3(H^+)}{c(Ce^{4+}) * c(Mn^{2+})}] = 0.88$$

During the discharging, the lower $[H^+]$ and higher $[Mn^{2+}]$ make the tendency of the conversion to MnOOH when the $\left[\frac{c(Ce^{3+}) * c^3(H^+)}{c(Ce^{4+}) * c(Mn^{2+})}\right] < 0.88, \Delta G < 0$.

Note:

① $\Delta_f G(MnOOH)$ is roughly assumed by the data and Hess's law [8].

② R: ideal gas constant (8.31 J K^{-1} mol^{-1}); T: temperature (25°C); Q: reaction entropy

References

1 Z. Shen, Z. Tang, C. Li, L. Luo, J. Pu, Z. Wen, Y. Liu, Y. Ji, J. Xie, L. Wang, Y. Yao and G. Hong, *Adv. Energy Mater.*, 2021, **11**, 2102055.

2 Y. Zeng, X. Zhang, Y. Meng, M. Yu, J. Yi, Y. Wu, X. Lu and Y. Tong, *Adv. Mater.*, 2017, **29**, 1700274.

3 H. Tang, W. Chen, N. Li, Z. Hu, L. Xiao, Y. Xie, L. Xi, L. Ni and Y. Zhu, *Energy Storage Mater.*, 2022, **48**, 335-343.

4 J. Gao, X. Xie, S. Liang, B. Lu and J. Zhou, *Nano-Micro Lett.*, 2021, **13**, 69.

5 J. Yang, G. Yao, Z. Li, Y. Zhang, L. Wei, H. Niu, Q. Chen and F. Zheng, *Small*, 2023, **19**, 2205544.

6 H. Dong, J. Li, S. Zhao, F. Zhao, S. Xiong, D. J. L. Brett, G. He and I. P. Parkin, *J. Mater. Chem. A*, 2020, **8**, 22637-22644.

7 S. Islam, M. H. Alfaruqi, V. Mathew, J. Song, S. Kim, S. Kim, J. Jo, J. P. Baboo, D. T. Pham, D. Y. Putro, Y.-K. Sun and J. Kim, *J. Mater. Chem. A*, 2017, **5**, 23299-23309.

8 L. C. Dong, Y. B. Zhong, S. Zhe, T. Y. Zheng and H. Wang, *RSC Adv.*, 2016, **6**, 21037-21042.